Journal of Biomolecular NMR **29:** 187–198, 2004.

Carbonyl carbon transverse relaxation dispersion measurements and ms-μs timescale motion in a protein hydrogen bond network

Rieko Ishima[a,*], James Baber[b], John M. Louis[b] & Dennis A. Torchia[a]
[a]*Molecular Structural Biology Unit, National Institute of Dental and Craniofacial Research and* [b]*Laboratories of Chemical Physics, National Institute of Diabetes and Digestive and Kidney Diseases, National Institutes of Health, Bethesda, Maryland 20892-4307, U.S.A.*

Received 31 October 2003; Accepted 17 December 2003

Key words: chemical exchange, conformational change, CPMG, NMR, R_2

Abstract

A constant-time, Carr–Purcell–Meiboom–Gill (CPMG) transverse relaxation, R_2, dispersion experiment for carbonyl carbons was designed and executed to detect μs-ms time-scale dynamics of protein backbone carbonyl sites. Because of the large (ca. 55 Hz) C_α-C' J-coupling, the carbonyl signal intensity is strongly modulated as the spacing between CPMG pulses is varied, in uniformly ^{13}C enriched proteins, unless care is taken to minimize the perturbation of the C_α magnetization by the CPMG pulses. CPMG pulse trains consisting of either a band-selective pulse, such as RE-BURP, or rectangular (with an excitation null in the C_α region of the spectrum) pulses were employed in order to minimize C' signal modulation by C_α-C' J-coupling. The performance of these types of CPMG refocusing pulses was assessed by computer simulation, and by comparing dispersion profiles measured for (1) uniformly [^{13}C,^{15}N, ^{2}H] (^{2}H at non-labile hydrogen sites) labeled, and (2) uniformly ^{15}N/selectively-$^{13}C'$ labeled samples of HIV-1 protease bound to a potent inhibitor, DMP323. In addition, because the uniformly $^{13}C/^{15}N/^{2}H$ labeled sample was well suited to measure ^{15}N and ^{1}H R_2 dispersion as well as $^{13}C'$ dispersion, conformational exchange in the inter subunit β-sheet hydrogen-bond network of the inhibitor-bound protease was elucidated using relaxation dispersion data of all three types of nuclei.

Introduction

Protein dynamics on the ms-μs time scale reflect conformational changes associated with catalysis and ligand binding, and are therefore of interest for understanding structure-function relationships of enzymes. CPMG relaxation dispersion experiments, that measure the nuclear spin transverse relaxation rate, R_2, as a function of the effective RF field strength, are well suited to detect protein dynamics on this time scale (Palmer et al., 2001). Recently, pulse sequences have been presented that measure R_2 relaxation dispersion of ^{15}N backbone amides, ^{13}C methyl groups, ^{15}N side-chain NH_2 groups, and amide protons (Ishima and Torchia, 2003; Mulder et al., 2001, 2002; Skrynnikov et al., 2001; Tollinger et al., 2001). These sequences utilize a relaxation compensation element (Loria et al., 1999), to average the relaxation of inphase and anti-phase magnetization components, in conjunction with a constant-time CPMG period, that enables efficient measurement of R_2 over a wide range of effective RF fields.

Measurements of R_2 dispersion of backbone amide ^{15}N and ^{1}H sites are useful to detect fluctuations of protein secondary structures because the chemical shifts of these nuclei are sensitive to changes in hydrogen bonding and in backbone dihedral angles (Ishima and Torchia, 2003). Although chemical shifts of backbone carbonyl carbons are also sensitive to such structural changes, accurate measurements of CPMG-based R_2 relaxation dispersion for C' sites have not yet been reported. The reasons for this are two-fold. First, in uniformly ^{13}C enriched proteins,

*To whom correspondence should be addressed. E-mail: rishima@dir.nidcr.nih.gov

Table 1. C′ CSA, C′-X dipolar and ^{15}N R_1 contributions to relaxation of $2C_YN_Z$

B_o	τ_m	Total[a]	C′CSA[b]	Dipolar R_2^c				
		R_T	R_2	C′-H_α	C′-H_N	C′-C_α	C′-^{15}N	$R_1(^{15}N)$[d]
(T)	(ns)	(s^{-1})	(s^{-1})	(s^{-1})	(s^{-1})	(s^{-1})	(s^{-1})	(s^{-1})
11.7	12.0[e]	15.5	11.4	0.9	1.1	0.6	0.2	1.3
18.8	12.0	32.2	29.0	0.9	1.0	0.6	0.2	0.5

[a]Total relaxation rate of $2C_YN_Z$ coherence, R_T, is the sum of R_2(C′ CSA), R_2(C′-X dipolar), and $R_1(^{15}N)$. The CSA and dipolar relaxation rates were calculated assuming isotropic overall motion and standard equations for R_2 that neglect internal motion and effects of dipolar/CSA cross correlation (Cavanagh et al., 1996).
[b]Calculated using the parameters $\Delta\sigma = 120$ ppm and $\eta = 0.73$ (Cornilescu and Bax, 2000).
[c]Heavy atoms are directly bonded to C′, and H atoms are separated from C′ by two bonds, so that the C′-H internuclear distances ($d_{C'-H\alpha} = 2.1$ Å, $d_{C'-HN} = 2.14$ Å) are independent of protein conformation. Conformation dependent, longer range dipolar C′-X interactions, where C′ and X are separated by at lease three bonds, are neglected because their contributions to R_T are ca. 10-fold smaller than the dipolar interactions considered.
[d]The $R_1(^{15}N)$ at 11.7 T is the average ^{15}N R_1 reported for the protease/DMP323 complex (Ishima et al., 1998), and the value listed at 18.8 T was calculated assuming that R_1 is proportional to B_o^{-2}.
[e]This is the overall correlation time of the protease under the conditions used herein (Ishima et al., 1998).

evolution of transverse C′ magnetization by the strong one bond C_α-C′ J-coupling, ca. 55 Hz, during the CPMG period must be suppressed in order to make accurate R_2 measurements. Second, the sensitivity of the C′ R_2 relaxation experiment is lower than that of the amide ^1H and ^{15}N experiments because of the decay of coherence that occurs during the two INEPT steps required for transfer of coherence of either ^{15}N or $^{13}C_\alpha$ spins to-and-from C′ spins.

Herein we report C′ R_2 dispersion measurements of the HIV-1 protease bound to an inhibitor, DMP323. Because chemical shift anisotropy (CSA) relaxation, the dominant source of C′ spin relaxation (Table 1), increases as the square of the static magnetic field strength, use of a magnetic field greater than 11.7 T (that corresponds to 500 MHz ^1H frequency) does not significantly increase the sensitivity of the C′ R_2 dispersion experiment. Therefore, in order to maximize sensitivity, spectra were recorded at 11.7 T using a cryoprobe (Bruker, Bellerica, MA).

C_α-C′ J-coupling artifacts were suppressed by using CPMG pulse trains composed of (a) either RE-BURP or (b) rectangular pulses, that selectively inverted the C′ spins while minimally perturbing the C_α spins. The effectiveness of these pulse trains in minimizing artifacts in the R_2 dispersion profiles was ascertained by (a) detailed numerical simulations and (b) by comparing R_2 C′ dispersion measurements made on a uniformly [^{13}C,^{15}N,^2H] labeled sample of the HIV-1 protease bound to the potent inhibitor DMP323, with results obtained using a sample that was uniformly ^{15}N labeled and selectively $^{13}C'$ labeled at a few types of amino acids. Because the uniformly [^{13}C,^{15}N,^2H] labeled sample was well suited for ^{15}N and ^1H R_2 measurements, R_2 dispersion profiles were obtained for all three spin types. These data were used to discuss the nature of the slow conformation fluctuations of the four-stranded β-sheet, which forms the primary inter-monomer interface of the protease homodimer.

Results and discussion

A Pulse sequence for measuring C′ R_2 dispersion

The pulse scheme used for the C′ R_2 dispersion experiment, Figure 1, employed HNCO-type coherence transfer to generate C′ transverse coherence. An HCACO-type approach was not used for two reasons. First, C_α-C_β INEPT-transfer efficiently competes with C_α-C′ transfer unless the C_β spins are selectively decoupled (Matsuo et al., 1996). Unfortunately, selective decoupling of the C_β spins perturbs C_α spins having chemical shifts that lie outside the 45–60 ppm range. Second, although the HCACO experiment is recorded in D_2O, so that the C′-H_N dipolar interaction does not contribute to the C′ R_2, this offers little advantage because CSA is the dominant C′ transverse relaxation mechanism (Table 1).

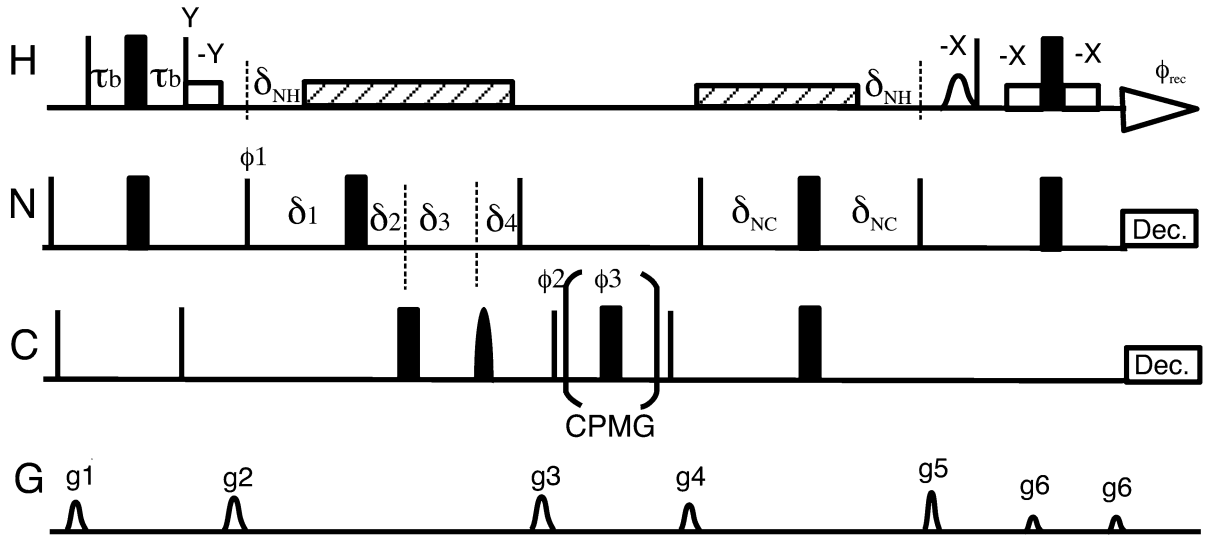

Figure 1. Pulse scheme of the carbonyl ^{13}C relaxation dispersion experiment. Narrow (wide) bars corresponding to 90° (180°) RF pulses were applied with phase x, unless indicated otherwise. Non-rectangular RF and gradient pulses had the shape of the first lobe of a sine function. All carbon pulses were applied with the RF carrier set to 175 ppm except for a carbon shaped pulse which was an off-resonance, 250 μs, 180° pulse applied at 55 ppm. All proton pulses were applied at the water resonance frequency, and the open squares represent 1 ms 180° rectangular pulses. Values of fixed delays were: $\tau_b = 2.7$ ms; $\delta_{NX} = 5.4$ ms. Initial values of the variable delays were: $\delta_1 = 13.5$ ms $+ \delta_2 + 56$ μs, and $\delta_3 + \delta_4 = 13.5$ ms, and $\delta_2 = \delta_4 = 4$ μs. Semi-constant-time evolution in t1 was achieved by incrementing δ_2 and δ_4 by $t_D/2$-α and $t_D/2$, respectively, and by decrementing δ_1 by α, where t_D is the dwell time in t_1 and α is δ_1 divided by number of t_1 points. The phase cycle was $\phi1 = \{x, x, -x, -x\}$, $\phi2 = \{x, -x\}$, $\phi3 = \{4(y), 4(-y)\}$, and $\phi_{receiver} = \{x, -x, -x, x\}$. All gradients were applied along z with maximum amplitude of 25 G/cm for g_1-g_5 and 7 G/cm for g_6. Gradient durations for g_1-g_6 were 1.0 ms, 1.1 ms, 1.4 ms, 1.3 ms, 1.4 ms, and 0.8 ms, respectively. The CPMG pulses were either (A) rectangular, or (B) 480 μs RE-BURP pulses. In the case of the uniformly ^{13}C enriched protein, the duration of the rectangular CPMG pulse was chosen so that an excitation null occurred in the C_α region of the spectrum, at either 50 or 60 ppm. The total length of the constant time CPMG period, T_{CP}, was 32 ms. During T_{CP}, from 2 to 128 pulses were applied, corresponding to effective B_1 fields ranging from 31.25 to 2000 Hz. For each t_1 increment, axial peaks were shifted to the edge of the spectrum by inversion of $\phi1$ in concert with the receiver phase (Marion et al., 1989). Note that at the beginning to the CPMG constant time period that the density operator is proportional to antiphase $2C_YN_Z$ coherence, rather than in-phase C_X coherence. However, as seen in Table 1, $R_2(C_{X,Y}) >> R_1(N_Z)$ so that $R_2(2C_YN_Z)$ is only slightly larger than $R_2(C_Y)$. Therefore R_2 measurements which use $2C_YN_Z$ coherence, rather than C_X coherence, at the beginning of the CPMG period have better sensitivity, because the pulse sequence in the latter case requires two additional C′-N INEPT elements.

Examination of Figure 1 reveals that the pulse sequence lacks a relaxation compensation element (Loria et al., 1999). Relaxation compensation was not applied because this approach (which would average the relaxation of inphase (C'_X) and antiphase ($2C'_YN_Z$) coherences) requires inclusion of two additional C′-N INEPT steps that reduce the sensitivity of the experiment. Fortunately, numerical simulations show that the error in the C′ R_2 measurement introduced by neglecting relaxation compensation is less than 1%, provided that $\tau_{CP} \leq 8$ ms. ($2\tau_{CP}$ is the time between the centers of CPMG refocusing pulses, and is related to the effective B_1 (RF) field strength in the rotating frame as $1/4\tau_{CP} = \nu_{CP}$). The error is small because (1) the relatively small N-C′ J-coupling (15 Hz) causes little interconversion of C'_X and $2C'_YN_Z$ coherence during the periods between CPMG refocusing pulses and (2) the ^{15}N longitudinal relaxation rate is over ten-fold smaller than the C′ transverse relaxation rate, Table 1. The restriction that $\tau_{CP} \leq 8$ ms implies that $T_{CP} \leq 32$ ms (which in turn implies that $\nu_{CP} \geq 31.25$ Hz), where T_{CP} is the total duration of the constant time CPMG period. Larger values of T_{CP} are achieved if $\tau_{CP} > 8$ ms, but at the cost of a significant reduction in sensitivity, particularly when conformational exchange contributes substantially to R_2.

As noted earlier, a pulse sequence that measures R_2 dispersion must suppress evolution of the density operator, ρ, during the CPMG (and relaxation compensation INEPT period, when present) period by homonuclear J-coupling. While homonuclear J couplings have negligible effects on amide ^{15}N dispersion measurements, they can have major impacts on measurements of ^{13}C and amide ^1H relaxation dispersion profiles (Ishima and Torchia, 2003; Mulder

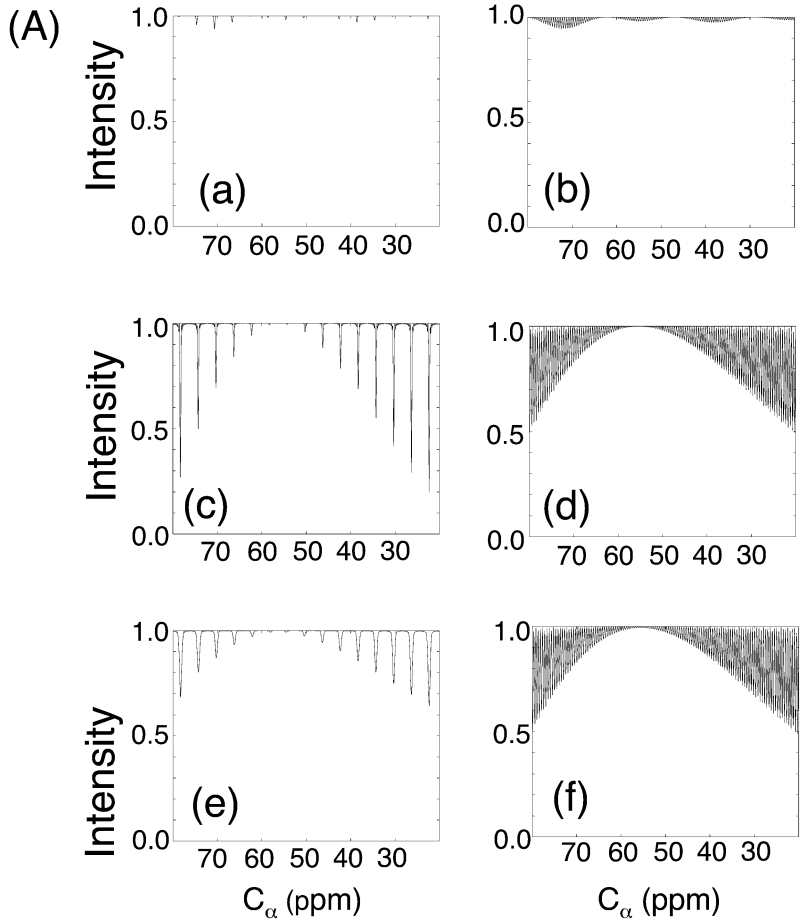

Figure 2. Numerical simulations showing the fraction of C'_Y coherence, $f_{C'Y} = <C'_Y(T_{CP}) >/< C'_Y(0)>$, that remains after 32 ms of CPMG evolution, plotted as a function of the chemical shift of the C_α spin that is J-coupled to the C' spin. The numerical procedure used to calculate f_T is described in Materials and methods. In the plots shown, the C' chemical shift and the carbon RF carrier were set at 173 and 175 ppm respectively. ν_{CP} was set either to 125 Hz (eight CPMG pulses during 32 ms T_{CP} period) in (a), (c), and (e), or to 31.25 Hz (two CPMG pulses) in (b), (d), and (f). In the simulation (a) and (b), 480 μs RE-BURP band selective refocusing pulses were used as CPMG pulses. In simulations (c) and (d), C' rectangular refocusing pulses have an excitation null at 55.0 ppm and B_1 RF fields are spatially homogeneous. In (e) and (f) the calculations are repeated using the same refocusing pulses as in (c) and (d) but using a spatially inhomogeneous B_1 field (modeling that of the NMR probe) having relative intensities of 0.84, 0.92, 1.0, 1.08, 1.16 (unit intensity corresponds to a 180° pulse) weighed with a 1:4:6:4:1 distribution (Geen and Freeman, 1991).

et al., 2002). In these cases, the introduction of RE-BURP pulses (band selective 180° refocusing pulses) into the CPMG and/or relaxation compensation elements of the pulse sequence significantly reduced the effects of homonuclear J-coupling on R_2 dispersion measurements.

In the case of the C' R_2 dispersion experiment performed on a uniformly ^{13}C enriched sample, the pulse sequence must suppress the net evolution of density operator terms that contain either C'_X or C'_Y operators, by the ca. 55 Hz C_α-C' J-coupling, during the CPMG period. CPMG pulses that selectively refocus only transverse C' coherence eliminate net evolution of ρ due to $^1J_{C\alpha-C'}$. Selective refocusing of C' spins can be achieved by either (1) band-selective RE-BURP pulses (Geen and Freeman, 1991) or (2) on-resonance C' rectangular pulses calibrated to produce a 360° rotation (null excitation) at the off-resonance C_α position (i.e., by setting $\sqrt{3}$ γB_1 equal to the difference in chemical shifts of the J-coupled C_α and C' spins (Cavanagh et al., 1996; Ernst et al., 1987)).

Numerical simulations of C'_Y evolution during the CPMG period

Evolution of C'_Y coherence during the CPMG period was numerically simulated, neglecting relaxation, as described in the Methods and materials. Figure 2 presents a comparison of profiles, $f_{C'Y}$, the fraction of $<C'_Y>$ ($<Q>$ is the expectation value of Q) that remains at the end of the CPMG period. $f_{C'Y}$ is plotted as a function of the chemical shift of the C_α spin, that is J-coupled to C', for CPMG pulse trains consisting of RE-BURP pulses, Figures 2a and b, and, rectangular refocusing pulses, Figures 2c and d. Ideally, if CPMG pulses applied to the C' spins do not perturb the C_α spins, the CPMG pulse train fully refocuses C'_Y coherence and $f_{C'Y}$ equals unity. Although the 480 μs RE-BURP pulses applied at 175 ppm are highly selective for the C' spins, they slightly perturb the C_α spins, which typically resonate in the 40–70 ppm range. As a consequence, C'_Y coherence need not completely refocus, because evolution due to C_α-C' J-coupling is not fully suppressed, resulting in a reduction in $f_{C'Y}$. Numerical simulations of 480 μs RE-BURP CPMG pulse trains applied at 175 ppm, Figures 2a and b, show that for C_α spins in the 40–70 ppm range, $f_{C'Y}$ is the range of 0.96–1.0, with pronounced local minima (dips) occurring at C_α chemical shift increments of $2\nu_{CP}$. In addition, as expected, based upon the excitation profile of the RE-BURP pulse, the deviation of $f_{C'Y}$ from unity decreases, with a periodic modulation, as the chemical shift difference between the C' and C_α spins increases, Figures 2a and b.

The dips in $f_{C'Y}$ are also observed when rectangular CPMG pulses, having a null inversion are used to calculate $f_{C'Y}$ profiles, Figures 2c and d. The null inversion of the rectangular pulse is at 55 ppm. Furthermore, as expected, the attenuation of $f_{C'Y}$ is minimal near 55 ppm, Figures 2c and d, and increases as the chemical shift of the C_α spin increasingly deviates from 55 ppm. As with the RE-BURP pulse train, dips in $f_{C'Y}$ occur at C_α chemical shift increments of $2\nu_{CP}$.

The simulations show that, as a consequence of the large C'-C_α J-coupling, the small perturbation of the C_α spins by the RE-BURP pulses, results in a predicted maximum reduction of 0.04 in $f_{C'Y}$, throughout the full C_α chemical shift range of 40–70 ppm, Figures 2a and b. The null-excitation rectangular pulse train performs as well as the RE-BURP pulse train, but only over a considerably smaller range of C_α chemical shifts, $\sim$ 10 ppm, Figures 2c and d. However, by recording two relaxation data sets with the rectangular CPMG pulses having null inversions at 60 ppm and 50 ppm, respectively, the reduction in $f_{C'Y}$ of no more than ca. 0.04 is obtained for C_α chemical shifts in the range of 45 to 65 ppm. Therefore, use of selective rectangular pulses yields relaxation data having accuracy comparable to that obtained using RE-BURP CPMG pulses, with the disadvantage that two experiments are required. An advantage of the rectangular pulse train (consisting of 100–120 μs 180° pulses) is that it achieved a value of ν_{CP} of 2kHz, twice the maximum attainable using 480 μs RE-BURP pulses, while depositing ca. the same amount of RF energy in the probe as the RE-BURP pulse train with $\nu_{CP} = 1$ kHz.

Effect of B_1 spatial inhomogeneity on R_2 measurements

The plots in Figures 2c and d were calculated assuming spatially homogeneous B_1 (RF) fields. This is, of course, an idealization. In the case of the cryoprobe employed to make the C' R_2 measurements, the observed transverse magnetization following an $810°_X$-pulse, $M_Y(810)$, was only ca. 60% of that following a $90°_X$-pulse, $M_Y(90)$, because of B_1 spatial inhomogeneity. In order to account for B_1 inhomogeneity in the numerical simulations, it was assumed that the intensity of the B_1 field applied during the CPMG pulse had relative values of 0.86, 0.93, 1.0, 1.07, 1.14 (where the B_1 field intensity having a relative value of unity corresponds to a 180° pulse) that were weighted by the binomial coefficients 1:4:6:4:1. This distribution of B_1 values reproduced the observed ratio, $M_Y(810)/M_Y(90) = 0.6$, and was therefore used to calculate Figures 2e and f. Comparison of these results with those in Figures 2c and d shows that the effect of spatial inhomogeneity of B_1 is to increase the width of the dips in $f_{C'Y}$ while reducing their magnitude. In addition, although it is not obvious in Figure 2, in the absence of chemical exchange, $f_{C'Y}$ is slightly less than unity for all values of the C_α chemical shift, because coherence of spins that do not experience 180° CPMG pulses (due to B_1 spatial inhomogeneity) is not perfectly refocused.

Error in C' R_2 measurements introduced by $^3J_{C'i-C'i\pm1}$ couplings and $^3J_{C'-C\gamma}$ couplings

Unlike the chemical shift of the C' and C_α spins, which are separated by ca. 120 ppm, the C' chemical shifts of the naturally occurring amino acid residues lie within a 10 ppm range (ca. 170–180 ppm). Therefore,

selective refocusing cannot be used to suppress evolution due to vicinal (three-bond) $^3J_{C'i-C'i\pm1}$ couplings. Although these couplings are usually quite small, typically less than 1.2 Hz in ubiquitin, one coupling of 2.3 Hz was observed (Hu and Bax, 1996). Calculations of $f_{C'Y}$, for C'_i, as a function of the chemical shift $C'_{i\pm1}$, were performed using the following parameters: $T_{CP} = 32$ ms, ν_{CP} in the range of 31.25 to 2000 Hz, and $^3J_{C'i-C'i\pm1} = 1.2$ or 2.5 Hz, C'_i and $C'_{i\pm1}$ chemical shifts in the range 170–180 ppm. As expected, evolution due to $^3J_{C'i-C'i\pm1}$ reduced the value of $f_{C'Y}$, leading to a small overestimate of R_2. The maximum overestimates in R_2 were found to be less than 0.3 s^{-1} and 1.2 s^{-1} for $^3J_{C'i-C'i\pm1} = 1.2$ and 2.5 Hz, respectively; therefore the error introduced in the R_2 dispersion measurement by $^3J_{C'i-C'i\pm1}$ coupling will typically be less that 0.5 s^{-1}. These errors are less than those calculated by Mulder and Akke (2003) for CPMG experiments, because the T_{CP} used in our simulations (32 ms) is over 3 times smaller than used in their simulations (100 ms). The value of T_{CP} used herein is appropriate for moderate to large proteins whereas the value used by Mulder and Akke (2003) is reasonable for small proteins.

Trans $^3J_{C'-C\gamma}$ couplings are significantly larger than $^3J_{C'i-C'i\pm1}$ couplings, attaining values of up to 5 Hz (Hu and Bax, 1996). Because C^γ chemical shifts of Asp and Asn (Asx) residues differ from C' chemical shifts by less than 15 ppm, selective refocusing cannot be used to suppress evolution due to $^3J_{C'-C\gamma}$, and a 5 Hz coupling can lead to overestimates in C' R_2 values of 5 s^{-1}. For the reason noted above, this error is less than that calculated by Mulder and Akke (2003). Even so, an error of in R_2 of 5 s^{-1} is significant. Therefore, C' R_2 dispersion observed using the CPMG approach for Asx sites in a uniformly labeled sample should be ascribed to conformational exchange only if $^3J_{C'-C\gamma}$ couplings are measured (Hu and Bax, 1996) and found to be small (less than ca. 2 Hz). Alternatively, if the $^3J_{C'-C\gamma}$ coupling is either large or cannot be measured, R_2 dispersion can be measured by the off-resonance $T_{1\rho}$ approach (Mulder and Akke, 2003) or by the CPMG approach in a sample selectively labeled at Asx C' sites. The CPMG and off-resonance $T_{1\rho}$ (Mulder and Akke, 2003) approaches are complimentary. In particular, because larger effective fields are used in the off-resonance $T_{1\rho}$ experiment, it is more sensitive to fast chemical exchange, τ_{ex} ($\approx 1/\gamma B_{eff}$) ca. 10^{-3} to 10^{-5} s, whereas the CPMG experiment is more sensitive to slower chemical exchange, τ_{ex} ca. 10^{-1} to 10^{-3} s.

Aromatic C^γ chemical shifts lie between 110 and 140 ppm (Hu et al., 1997). The relatively wide range of aromatic C^γ chemical shifts and their proximity to the C' shifts preclude using selective rectangular pulses to suppress evolution due to aromatic $^3J_{C'-C\gamma}$ coupling. Fortunately however, RE-BURP pulses can be used for this purpose, provided that the carrier frequency is set to ca. 190 ppm. Simulations show that when the carrier is at 190 ppm that the reduction of $f_{C'Y}$ is less than 3% for aromatic C_γ chemical shifts between 100 and 140 ppm. When the C' carrier offset is large it is desirable to minimize off-resonance effects. This can be achieved by making the durations of the rectangular ^{13}C 90° pulses that flank the CPMG period as short as possible (i.e., 15 μs or less). In addition inserting a pair of delay periods (each equal to $2\tau_{90}/\pi$, see equation 3.66 (Cavanagh et al., 1996)) between every pair of CPMG 180° pulses, will compensate for the offset dependent phase shifts introduced by the 90° pulse durations. Alternatively, this compensation can be achieved by reducing the durations of the initial and final CPMG periods by $2\tau_{90}/\pi$.

Finally we note that $^3J_{C'-C\beta}$ and $^3J_{C'-C\gamma}$ couplings involving aliphatic C_β and C_γ spins lie in the 0.5 to 4.5 Hz range. However these spins are separated from the C' spins by 100–170 ppm and the simulations show that both the selective rectangular and the band selective RE-BURP pulses effectively eliminate the effects of their small J couplings on C' evolution during the CPMG period.

Comparison of R_2 values obtained for the specifically and uniformly C' labeled HIV protease samples

To test whether the two types of CPMG pulses discussed above suppress the effect of C_α-C' J-coupling, C' relaxation dispersion profiles obtained for the uniformly $^{13}C'$ enriched HIV-protease sample were compared with profiles measured for the protease that contained specific types of C' enriched amino acids. In these latter samples, the C_α-C' ^{1}J-couplings are absent for all C' sites. In addition, for most C' sites that were compared, at least one, and often both, of the two possible $^3J_{C'i-C'i\pm1}$ couplings were absent in the specifically labeled samples. Thus, comparison of the dispersion profiles of the uniformly and specifically labeled samples also monitors the effect of the $^3J_{C'i-C'i\pm1}$ coupling on the R_2 measurement.

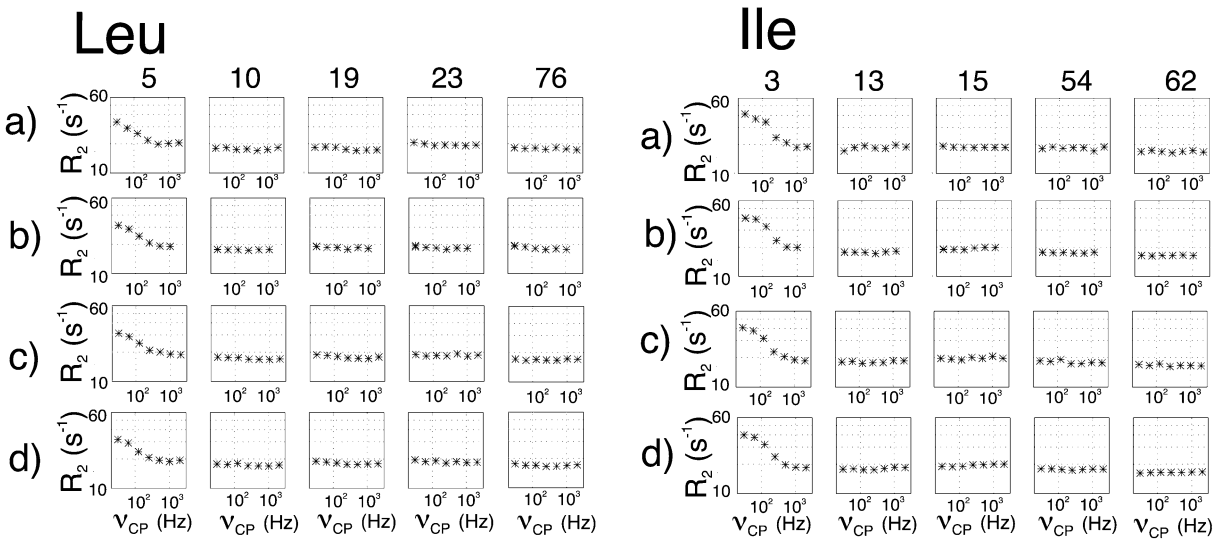

Figure 3. Comparison of C′ relaxation dispersion data of Leu and Ile residues measured using C′ selectively labeled and uniformly ^{15}N labeled samples, (a), and those measured using the ^{2}H, ^{13}C, ^{15}N uniformly labeled sample, (b), (c) and (d), of HIV-protease bound to DMP323. The three- letter code at the top left of each set of relaxation profiles identifies the type of amino acid, and the number identifies the location of the amino acid in the protease sequence. For each residue, the relaxation profiles were acquired with the RF carrier set at 175 ppm and (a) rectangular CPMG pulses; (b) 480 μs RE-BURP CPMG pulses; (c) 55.2 μs rectangular CPMG pulses with excitation null at 50 ppm; (d) 60.0 μs rectangular CPMG pulses with excitation null at 60 ppm.

Comparison of panels (a) and (b) in Figure 3 shows that R_2 dispersion profiles of Leu and Ile residues measured using selectively C′ labeled samples, Figure 3a, are essentially the same as those measured using the uniformly ^{13}C labeled protease sample and RE-BURP CPMG pulses, Figure 3b. For example, both panels (a) and (b) in Figure 3 reveal significant R_2 dispersion for Leu 5 and Ile 3, but no R_2 dispersion for other Leu and Ile residues. Similar results are seen in the case of Leu and Ile residues for the uniformly labeled sample when the CPMG trains consist of rectangular pulses with null excitation at 50 and 60 ppm, Figures 3c and d, respectively.

In similar fashion, R_2 dispersion profiles of Gly and Pro residues measured using selectively C′ labeled samples, Figure 4a, are essentially the same as those measured using the uniformly ^{13}C labeled protease sample and RE-BURP CPMG pulses, Figure 4b. On the other hand, the profiles observed for Gly residues using a uniformly labeled sample and a rectangular train with null excitation at 60 ppm, Figure 4d Gly profiles, show considerably larger fluctuations in R_2 as a function of ν_{CP}, than do the other Gly dispersion profiles, Figures 4a–c. This observation is reasonable because the Gly C_α spins typically resonate ca. 15 ppm upfield from the 60 ppm excitation null and are therefore significantly perturbed by the rectangular pulse train. In contrast with Gly C_α spins, Pro C_α spins typically resonate in the 60–66 ppm range. Therefore proline profiles exhibit significant spurious dispersion when the rectangular CPMG pulses have null excitation at 50 ppm, Figure 4c, but not when the null excitation is at 60 ppm, Figure 4d.

^{1}H, ^{15}N, $^{13}C'$ *relaxation dispersion*

Backbone amide ^{1}H, ^{15}N, and carbonyl ^{13}C relaxation dispersions were measured for the uniformly labeled D25N protease sample bound to a potent inhibitor, DMP323. The inhibitor bridges the two monomers at the active site resulting in the formation of a tight ternary complex at the protein concentration used in the NMR experiments, in spite of the fact that the D25N mutation increases the free dimer dissociation constant by ca. 1000 fold as compare to the wild-type (Louis et al., 2003). The major dimer interface not involving the inhibitor is a 4-stranded anti-parallel β-sheet consisting of residues 1-4 and 96-99 of each monomer. Previous studies of the active protease bound to DMP323 have indicated significant ms-μs motion in this interfacial β-sheet and in the adjacent N-terminal loop (residues 5-7) (Ishima et al., 1999; Ishima and Torchia, 2003).

The C′ relaxation dispersion data obtained in this study complement those of ^{15}N and ^{1}H. As seen in

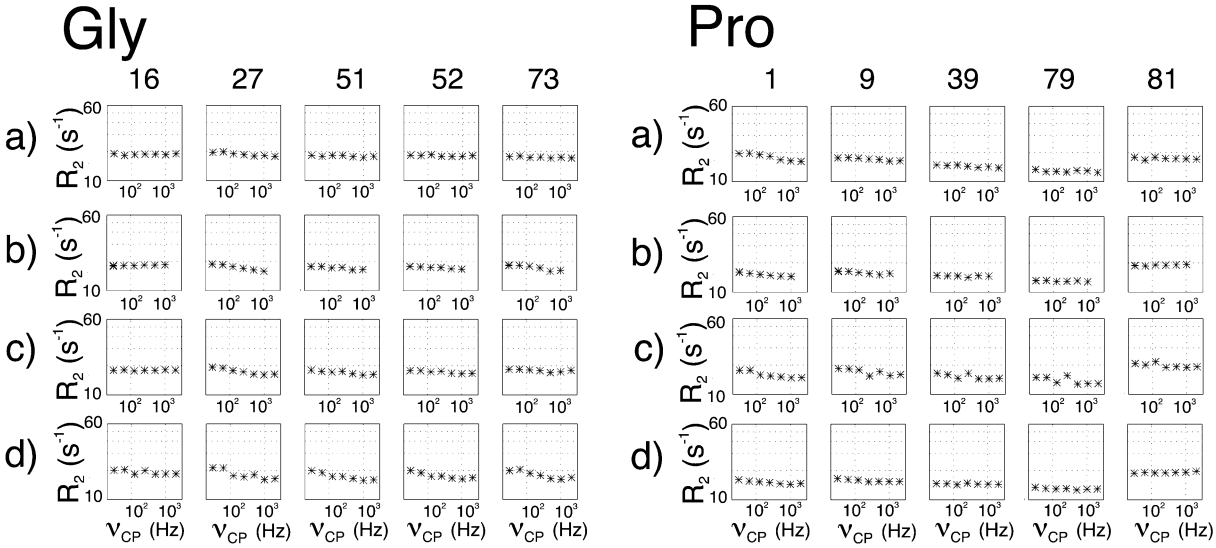

Figure 4. Comparison of C′ relaxation dispersion data of Gly and Pro residues measured using C′ selectively labeled and uniformly ^{15}N labeled samples, (a), and those measured using the ^{2}H, ^{13}C, ^{15}N uniformly labeled sample, (b), (c) and (d), of HIV-protease bound to DMP323. Conditions used to obtain the relaxation profiles are those provided in the caption of Figure 3.

Figure 5, ^{1}H, ^{15}N and ^{13}C relaxation dispersion is observed for residues 2-8 and 96-99, although the dispersion amplitudes vary from one spin type to the next. In addition, note that the amide dispersion of residue (i) is better correlated with the C′ dispersion of residue (i−1) than of residue (i). This result is expected because the peptide bond connects the C′ of residue (i−1) with the amide N of residue (i), Figure 6.

Further examination of Figure 6 shows that the spins of amide and carbonyl hydrogen bond partners, 96CO-HN98′ and 97CO-HN97′ in the two C-terminal inner strands of the sheet, display significant relaxation dispersion, Figure 5. The observation is consistent with ms-μs timescale motion of the C-terminal strands detected in a previous methyl dynamics study (Ishima et al., 2001). Dynamics between the C-terminal and N-terminal strands is also evident in Figures 5 and 6. The spins of all three H, N, C′ atoms of 3CO-97′HN hydrogen bond show relaxation dispersion curves, as do the C′ and N spins of the atoms of the 97′CO-3HN and 1CO-99HN hydrogen bonds.

It is noteworthy that the R_2 of Asn 98 oscillates as a function of ν_{CP} (Figure 5). This is most likely due to the effect of $^{3}J_{C'-C\gamma}$ coupling. Although the Asn 98 side chain is exposed to solvent, the chemical shifts of its β-protons are not degenerate. Therefore, Asn 98 may have restricted mobility resulting in a $^{3}J_{C'-C\gamma}$ coupling exceeding 2 Hz.

In the previous study of the active protease/DMP323 complex (Ishima and Torchia, 2003), small but clear ^{1}H relaxation dispersion was observed for residues 3 and 99. In contrast, in the inactive protease/DMP323 complex, amide ^{1}H relaxation dispersion is not evident for residues 3 and 99, Figure 5). We note that, in addition to the D25N mutation the inactive protease construct also contains a V3I mutation. The later mutation does not affect the enzymatic activity, but affects the chemical shifts of residue 3 and neighboring residues. Also, the V3I mutation leads to some repositioning of the hydrophobic sidechains within the interior of the terminal dimer interface, which we suspect, results in slight change of the average orientation of the aromatic ring of Phe 99. The resulting differences in ring currents at the amide sites of the two protease constructs would then cause differences in the ^{1}H, but not ^{15}N relaxation dispersion (Ishima et al., 1998), as is observed, Figure 5.

The data in Figure 5 clearly confirm previous observations that there is a significant conformational fluctuation of the dimer interface of the protease on the ms-μs timescale. Structural data (NOESY, chemical shift, hydrogen exchange) strongly indicate that, the conformation of the major species in solution is very similar to that observed in crystals (Yamazaki et al., 1996). The conformation of the minor (invisible) species is unknown, but of great interest, because it may provide insights into aspects of protease function

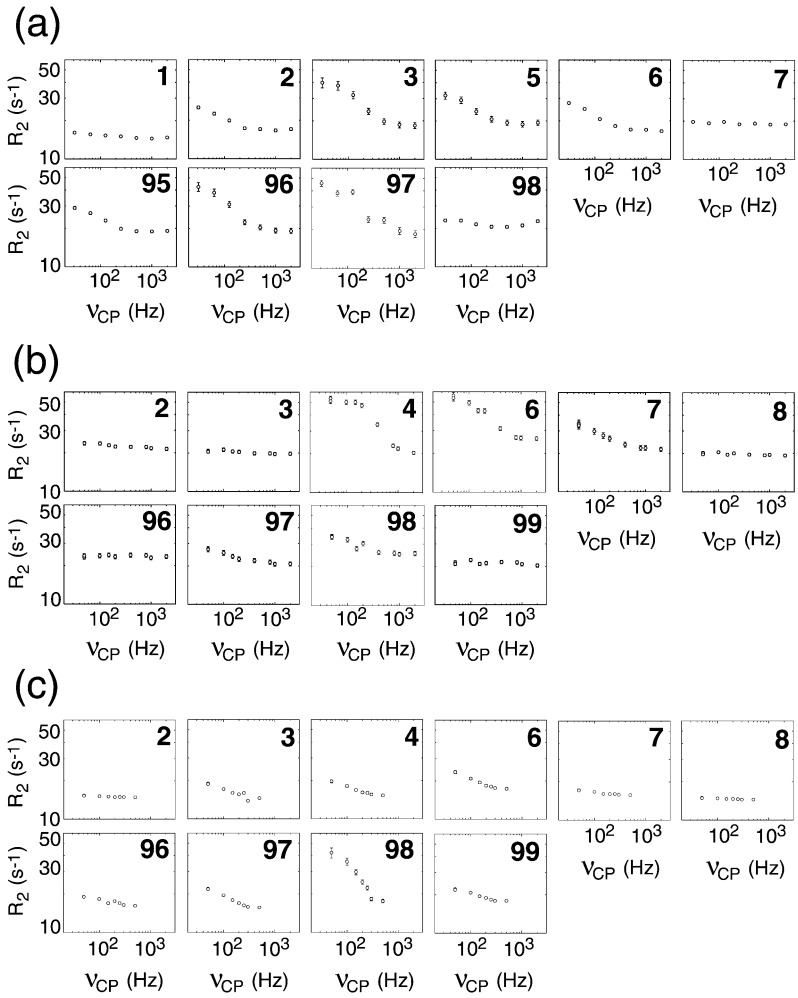

Figure 5. Comparison of R_2 relaxation profiles obtained for (a) carbonyl ^{13}C, (b) amide ^{1}H and (c) amide ^{15}N sites in residues in the interfacial β-sheet and the adjacent loop regions of the inactive HIV-1 protease bound to DMP323. Because the peptide bond directly links the C′ atom to the amide ^{15}N in the succeeding residue, each C′ relaxation profile is placed in the same column as the amide profile of the succeeding residue to facilitate comparison of conformational exchange at these neighboring sites.

related to dimer formation, maturation and autocatalysis. Recently developed relations correlating ^{1}H, ^{13}C and ^{15}N chemical shifts with protein structure (Neal et al., 2003) provide a promising approach for determining structures of minor species if their chemical shifts can be obtained. Although the signals of the minor protease species are not directly observed in the R_2 dispersion experiments, their chemical shifts can be obtained from a combination of field-dependent R_2 dispersion and HSQC experiments (Millet et al., 2000; Skrynnikov et al., 2002). Therefore the data provided by R_2 dispersion experiments for three types of backbone spins hold promise for providing information about elusive minor conformations of proteins. In particular, the protease dispersion data are currently being used identify the structure of the minor species of the dimer interface as well as to determine rate of exchange of minor and major interface conformations.

Materials and methods

NMR samples

HIV-1 protease (MW ca. 22 kDa, as a dimer) having the active site mutation, D25N, bound to inhibitor DMP323 was prepared as described previously (Louis et al., 2002). This inactive D25N mutant exhibits the same fold as that of the wild type protease (Katoh

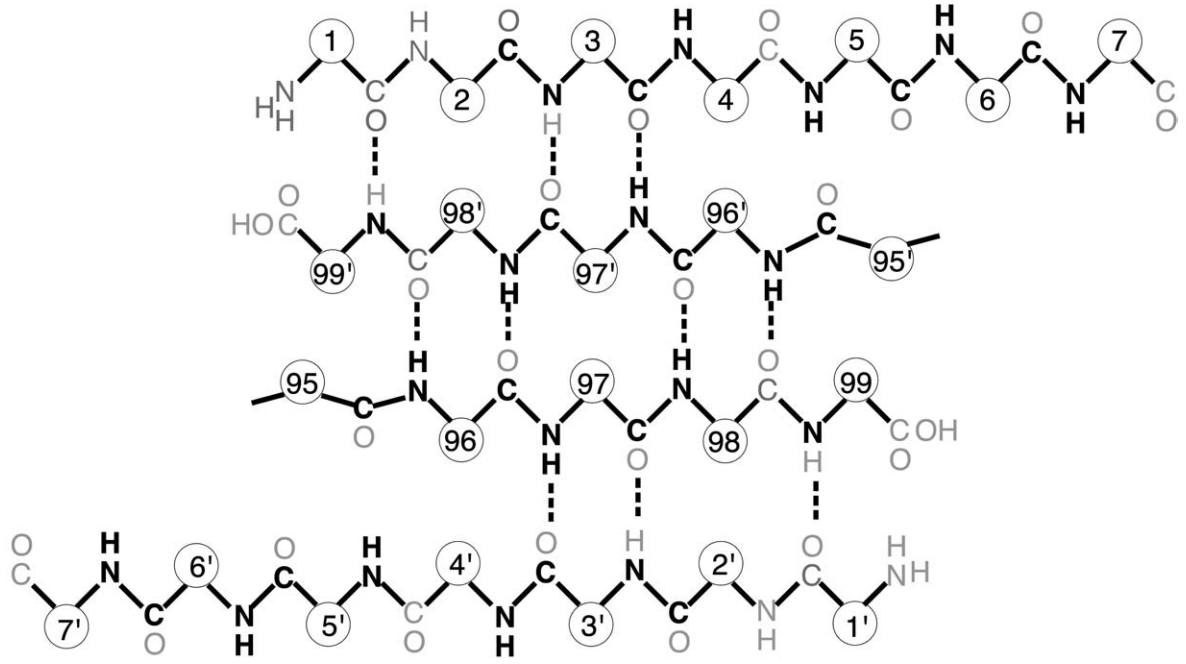

Figure 6. Secondary structure and β-strand topology of the terminal β-sheet (residues 1-4, 96-99) and adjoining N-terminal loop (residues 4-7) regions of the HIV-protease. The four-stranded β-sheet is the primary intermonomer interface of the protease homodimer, and contains an N- and C-terminal β-strand from each monomer (primed numbers identify amino acid residues in the second monomer subunit). Because DMP323 is a two-fold symmetric inhibitor, the protease/DMP323 complex has two-fold symmetry, and nuclei in residues numbered i and i′ have indistinguishable chemical shifts and relaxation rates. In the drawing, boldface letters identify C, N, H sites that undergo conformational exchange. Grey letters indicate sites for which data were not measured, such as oxygen spins, or were not detected because of overlapping signals. The amide H and N atoms of Leu 5 are shown in bold because their signals were severely broadened by conformational exchange, herein and in a previous study (Ishima et al., 1999).

et al., 2003) and is devoid autoproteolysis, which reduces protein yield and results in the gradual accumulation of peptide fragments (autoproteolysis products) as seen for wild type protease. The inactive protease contains an Ile a position 3 whereas the PR construct contains a Val at position 3. This is a minor difference in sequence which is commonly observed in wild-type variants of the protease, as we discuss in the Results and discussion. In order to measure ^{1}H, ^{13}C and ^{15}N R_2 dispersion profiles using a single sample, a sample was uniformly labeled with ^{2}H, ^{13}C and ^{15}N by using M9 medium containing 99.8% D_2O, uniformly [^{2}H,^{13}C]-glucose and ^{15}N-ammonium chloride. Two additional samples were prepared that were uniformly ^{15}N enriched, but specifically ^{13}C labeled at only the carbonyl position (to eliminate C_α-C′ and C'_i-$C'_{i\pm1}$ J-couplings) of certain types of amino acids. These samples were prepared using M9 medium containing ^{15}N-ammonium chloride and either (I) [1-^{13}C]Ile or (II) [^{15}N, 1-^{13}C]Gly, [^{15}N, 1-^{13}C]Leu, and [1-^{13}C]Pro. The specifically labeled amino acids were added to the M9 medium prior to induction. The level of ^{13}C′ labeling in the protease was greater than 90% for Ile, Leu and Pro, and 70–80% for Gly. The only observable scrambling of the ^{13}C′ label was to the C′ of Ser37, Trp6 and Trp41 in the protease sample labeled with [1-^{13}C](Gly, Leu, Pro), presumably due to the metabolic transformation of the labeled Gly precursor to Ser and hence to Trp (Stryer, 1995).

R_2 relaxation dispersion measurements

Protein samples were maintained in 20 mM sodium phosphate buffer (pH 5.8, 95%H_2O/5%D_2O) at a concentration of 0.5 mM. All experiments were performed using Bruker DMX500 spectrometers at 20 °C. The C′ and amide ^{15}N relaxation dispersion experiments were recorded using a cryoprobe, while the amide ^{1}H relaxation dispersion experiment was recorded using an ambient temperature probe. Relaxation dispersion profiles were generated by measuring R_2 as a function of ν_{CP} (equal to 1/4 of the spacing between the centers of the CPMG pulses, τ_{CP}), the effective B_1 RF field applied during a constant CPMG period, T_{CP}.

Each R_2 value was determined from the ratio of two signal intensities, I_0, measured without the CPMG period, and I_{CP}, measured with a constant-time total CPMG duration, T_{CP}. For C′ relaxation dispersion experiments, T_{CP} was 32 ms and ν_{CP} was 31.25, 63.5, 125, 250, 500, 1000, 2000 Hz, except when using the 480 μs CPMG RE-BURP pulse, for which the maximum value of ν_{CP} was 1000 Hz. The ^{13}C RF carrier was set at 175 ppm, and the length of the rectangular pulses CPMG pulses were 55.2 μs and 60.0 μs in order to provide excitation null points at 50 ppm and 60 ppm respectively. The data presented in Figure 1 were derived from spectra recorded with 100 and 1024 complex points for F_1 and F_2 dimensions and with 32 scans per point.

Amide ^{1}H and ^{15}N relaxation compensated R_2 dispersion experiments were performed as described previously (Ishima and Torchia, 2003). The ^{1}H and ^{15}N 90° rectangular pulse widths were 10 μs and 50 μs, respectively. Proton pulses were applied at the water resonance except during the proton CPMG period where the rf carrier position was switched to either 8.3 or 8.5 ppm. ^{15}N 90° pulses were applied at 117 ppm. Spectra were recorded with $T_{CP} = 40$ ms and ν_{CP} equal to 50, 100, 150, 200, 400, 800, 1000, 2000 Hz and 50, 100, 150, 200, 250, 300, 500 Hz for ^{1}H and ^{15}N spins, respectively. The proton relaxation dispersion spectra were recorded with 128 and 1024 complex points for F_1 and F_2 dimensions and with 32 scans per point. The ^{15}N relaxation dispersion spectra were recorded with 100 and 1024 complex points for F_1 and F_2 dimension and with 16 scans per point.

The fractional error in R_2 due to random noise was estimated using the expression $fR_2 = (\delta_e/I_0)(1 + (I_0/I_{CP})^2)^{1/2}/(R_2T_{CP})$ where δ_e is the rms noise measured in the reference spectrum. Typically errors in the C′ R_2 measured at 500 MHz were less than 5% for R_2 less than 20 s^{-1}, and are shown for all three types of spins in Figure 4. Data analyses were performed using NMRPipe and NMRdraw software (Delaglio et al., 1995; Garrett et al., 1991).

Numerical simulations of density operator evolution during the constant time CPMG period

The time evolution of ρ during the CPMG period was calculated disregarding relaxation using the Liouville-Von Neumann equation. The numerical computation was carried out using MATLAB (Mathworks Inc., MA) as a sequence of unitary transformations (matrix multiplications) using (segmentally) time-independent Hamiltonians consisting of terms for (a) C′ and C_α chemical shift precession, (b) C_α-C′ J-coupling (55 Hz) and (c) CPMG pulses as propagators, with $\rho(0) = C'_Y$ (Ernst et al., 1987). Although ρ is actually proportional to C'_YN at the start of the CPMG period, N_z does not evolve under the action of the Hamiltonian, and it was sufficient to calculate the evolution of C'_Y. In all calculations, T_{CP}, was set to 32 ms, the value used in the experiments while the C′ and C_α chemical shifts were varied from 170–195 ppm and from 20 to 80 ppm, respectively. These large chemical shift ranges were used to insure that the calculations would cover all possible C′ and C_α chemical shifts encountered in experiments. CPMG pulse trains consisted of either RE-BURP or rectangular pulses. The RE-BURP pulse consisted of 256 rectangular elements and had a pulse width of 480 μs, corresponding to a 13 kHz maximum B_1 field strength. The 180° rectangular pulse width was in the range of 55–60 μs, with the value set by the desired null-excitation point in the C_α region of the spectrum. The values of ν_{CP} were set to those used in the experiments, i.e., 31.25, 62.5, 125, 250, 500, 1000 and 2000 Hz. In addition to calculations performed assuming homogeneous B_1 fields, simulations were also performed using a variety of distributions of B_1 fields that modeled the B_1 spatial inhomogeniety of the NMR probe, i.e. yielded a ratio: $M_Y(810)/M_Y(90) = 0.6$. The results of the calculations were displayed as profiles in which the ratio $f_{C'Y} = <C'_Y(T_{CP})>/<C'_Y(0)>$, where <Q> designates expectation value of Q, were plotted as a function of the chemical shift of the J-coupled C_α spin.

The calculations were slightly modified to simulate the effect of $^3J_{C'i-C'i\pm1}$ coupling on $f_{C'Y}$, by replacing the 55 Hz C_α-C′ J-coupling with $^3J_{C'i-C'i\pm1}$ couplings that varied from 1–6 Hz and employing C'_i and $C'_{i\pm1}$ chemical shifts that varied from 170 to 180 ppm.

Acknowledgement

This work was supported by the Intramural AIDS Targeted Anti-Viral Program of the Office of the Director of the National Institutes of Health.

References

Cavanagh, J., Fairbrother, W.J., Palmer, r., A.G. and Skelton, N.J. (1996) *Protein NMR Spectroscopy*, Academic Press, San Diego, pp. 135.

Cornilescu, G. and Bax, A. (2000) *J. Am. Chem. Soc.*, **122**, 10143–10154.

Delaglio, F., Grzesiek, S., Vuister, G.W., Zhu, G., Pfeifer, J. and Bax, A. (1995) *J. Biomol. NMR*, **6**, 277–293.

Ernst, R.R., Bodenhausen, G. and Wokaun, A. (1987) *Principles of Nuclear Magnetic Resonance in One and Two Dimensions*, Clarendon Press, Oxford.

Garrett, D.S., Powers, R., Gronenborn, A.M. and Clore, G.M. (1991) *J. Magn. Reson.*, **95**, 214–220.

Geen, H. and Freeman, R. (1991) *J. Mag. Reson.*, **93**, 93–141.

Hu, J.S. and Bax, A. (1996) *J. Am. Chem. Soc.*, **118**, 8170–8171.

Hu, J.S., Grzesiek, S. and Bax, A. (1997) *J. Am. Chem. Soc.*, **119**, 1803–1804.

Ishima, R., Freedberg, D.I., Wang, Y.X., Louis, J.M. and Torchia, D.A. (1999) *Structure*, **7**, 1047–1055.

Ishima, R., Louis, J.M. and Torchia, D.A. (2001) *J. Mol. Biol.*, **305**, 515–521.

Ishima, R. and Torchia, D.A. (2003) *J. Biomol. NMR*, **25**, 243–348.

Ishima, R., Wingfield, P.T., Stahl, S.J., Kaufman, J.D. and Torchia, D.A. (1998) *J. Am. Chem. Soc.*, **120**, 10534–10542.

Katoh, E., Louis, J.M., Yamazaki, T., Gronenborn, A.M., Torchia, D.A. and Ishima, R. (2003) *Protein Sci.*, **12**, 1376–1385.

Loria, J.P., Rance, M. and Palmer, A.G. (1999) *J. Am. Chem. Soc.*, **121**, 2331–2332.

Louis, J.M., Ishima, R., Nesheiwat, I., Pannell, L.K., Lynch, S.M., Torchia, D.A. and Gronenborn, A.M. (2003) *J. Biol. Chem.*, **278**, 6085–6092.

Marion, D., Ikura, M., Tschudin, R. and Bax, A. (1989) *J. Magn. Reson.*, **85**, 393–399.

Matsuo, H., Kupce, E., Li, H.J. and Wagner, G. (1996) *J. Magn. Reson. Ser. B.*, **113**, 91–96.

Millet, O., Loria, J.P., Kroenke C.D. and Palmer A.G. (2000) *J. Am. Chem. Soc.*, **122**, 2867–2877.

Mulder, F.A.A. and Akke, M. (2003) *Magn. Reson. Chem.*, **41**, 853–865.

Mulder, F.A.A., Hon, B., Mittermaier, A., Dahlquist, F.W. and Kay, L.E. (2002) *J. Am. Chem. Soc.*, **124**, 1443–1451.

Mulder, F.A.A., Skrynnikov, N.R., Hon, B., Dahlquist, F.W. and Kay, L.E. (2001) *J. Am. Chem. Soc.*, **123**, 967–975.

Neal, S., Nip, A.M., Zhang, H. and Wishart, D.S. (2003) *J. Biomol. NMR*, **26**, 215–240.

Palmer, A.G., Kroenke, C.D. and Loria, J.P. (2001) *Meth. Enzymol.*, **339**, 204–238.

Skrynnikov, N.R., Dahlquist, F.W. and Kay, L.E. (2002) *J. Am. Chem. Soc.*, **124**, 12352–12360.

Skrynnikov, N.R., Mulder, F.A.A., Hon, B., Dahlquist, F.W. and Kay, L.E. (2001) *J. Am. Chem. Soc.*, **123**, 4556–4566.

Stryer, L. (1995) In *Biochemistry*, W.H. Freeman and Company, New York, pp. 713–738.

Tollinger, M., Skrynnikov, N.R., Mulder, F.A.A., Forman-Kay, J.D. and Kay, L.E. (2001) *J. Am. Chem. Soc.*, **123**, 11341–11352.

Yamazaki, T., Hinck, A.P., Wang, Y.X., Nicholson, L.K., Torchia, D.A., Wingfield, P., Stahl, S.J., Kaufman, J.D., Chang, C.H., Domaille, P.J. and Lam, P.Y. (1996) *Protein Sci.*, **5**, 495–506.